How to cite: *Angew. Chem. Int. Ed.* **2020**, *59*, 12674–12679
International Edition: doi.org/10.1002/anie.202000712
German Edition: doi.org/10.1002/ange.202000712

Dendrimers

Single-Crystalline Optical Microcavities from Luminescent Dendrimers

Kohei Iwai, Hiroshi Yamagishi, Colin Herzberger, Yuji Sato, Hayato Tsuji, Ken Albrecht, Kimihisa Yamamoto, Fumio Sasaki, Hiroyasu Sato, Aswin Asaithambi, Axel Lorke, and Yohei Yamamoto**

Abstract: *Microcrystallites are promising minute mirrorless laser sources. A variety of luminescent organic compounds have been exploited along this line, but dendrimers have been inapplicable owing to their fragility and extremely poor crystallinity. Now, a dendrimer family that overcomes these difficulties is presented. First-, second-, and third-generation carbazole (Cz) dendrimers with a carbon-bridged oligo(phenylenevinylene) (COPV2) core (GnCOPV2, n = 1–3) assemble to form microcrystals. The COPV2 cores align uni/bidirectionally in the crystals while the Cz units in G2- and G3COPV2 align omnidirectionally. The dendrons work as light-harvesting antennas that absorb non-polarized light and transfer it to the COPV2 core, from which a polarized luminescence radiates. Furthermore, these crystals act as laser resonators, where the lasing thresholds are strongly coupled with the crystal morphology and the orientation of COPV2, which is in contrast with the conventional amorphous dendrimers.*

Luminescent organic microcrystallites are attractive minute laser sources that have been thoroughly investigated since the early stage of laser science.[1–8] Their luminescent properties can be readily modulated by modifying the π-conjugation of the constituent dye molecules or deforming the macroscopic morphology of the crystallites. Well-aligned transition dipoles of the constituent molecules and flat end facets of microcrystals are advantageous in enhancing their optical gain and suppressing radiation leakage.[9] To date, applications of microcrystal lasers cover diverse optics fields including full-color displays,[10] single-mode lasing,[11–13] phototransistors,[14] and photo energy conversion.[15]

Among the vast family of organic laser dyes, dendrimers are one of the highly promising classes.[16] Dendrimers are compositionally discrete macromolecules having multi-branched dendrons in vicinity to the central core. By virtue of their high solubility, high quantum yields, light harvesting potential, and remarkable tolerance toward luminescent quenching upon solidification, dendrimers have been utilized for research on photophysics and photochemistry.[17,18]

Lasing from dendrimers has been achieved in solution and in the amorphous solid state by incorporating them into certain optical cavities such as photonic crystal resonators[19,20] and distributed Bragg reflectors.[21,22] However, fabrication of crystalline optical microcavities from dendrimers still remains a formidable challenge, owing to their fragility and poor crystallinity. The sterically bulky morphology and the prominent conformational flexibility of the dendrons make the orderly packed crystalline state quite unfavorable both entropically and enthalpically. Although there are several reports highlighting crystalline dendrimers,[23,24] they are usually quite fragile and readily degrade upon evaporation of the included solvents. Therefore, dendrimers in the crystalline state have rarely been utilized for laser applications, which requires sufficiently stable materials against photo and thermal stimuli. Ideal dendrimer crystals with certain robustness would be attractive in the field of optics

[*] K. Iwai, Dr. H. Yamagishi, Prof. Y. Yamamoto
Department of Materials Science,
Faculty of Pure and Applied Sciences, and
Tsukuba Research Center for Energy Materials Science (TREMS)
University of Tsukuba, 1-1-1 Tennodai
Tsukuba, Ibaraki 305-8573 (Japan)
E-mail: yamagishi.hiroshi.ff@u.tsukuba.ac.jp
yamamoto@ims.tsukuba.ac.jp

C. Herzberger, Y. Sato, Prof. H. Tsuji
Department of Chemistry, Faculty of Science, Kanagawa University
2946 Tsuchiya, Hiratsuka 259-1293 (Japan)

C. Herzberger
Institute of Organic Chemistry, Clausthal University of Technology
Adolph-Roemer-Straße 2A, 38678 Clausthal-Zellerfeld (Germany)

Prof. K. Albrecht, K. Yamamoto
Laboratory for Chemistry and Life Science
Tokyo Institute of Technology
4259 Nagatsuta Midori-ku, Yokohama 226-8503 (Japan)
and
ERATO Yamamoto Atom Hybrid Project
Japan Science and Technology Agency (JST)
4259 Nagatsuta Midori-ku, Yokohama 226-8503 (Japan)

Prof. K. Albrecht
Institute for Materials Chemistry and Engineering, Kyushu University
6-1 Kasuga-koen, Fukuoka 816-8580 (Japan)

Dr. F. Sasaki
Electronics and Photonics Research Institute, National Institute of Advanced Industrial Science and Technology (AIST)
1-1-1 Umezono, Tsukuba, Ibaraki 305-8568 (Japan)

Dr. H. Sato
Rigaku Corporation
12-9-3 Matsubara, Akishima, Tokyo 196-8666 (Japan)

A. Asaithambi, Prof. A. Lorke
Faculty of Physics and CENIDE, University of Duisburg-Essen
Lotharstraße 1, 47057 Duisburg (Germany)

Supporting information and the ORCID identification number(s) for the author(s) of this article can be found under: https://doi.org/10.1002/anie.202000712.

and materials science, because single-crystalline state makes both chemical and physical properties spatially anisotropic.

Recently, we reported a π-conjugated dendrimer that partially overcomes these difficulties.[25] We have been focusing on a series of carbazole (Cz) dendrimers[26] with the aim of enhancing their light-harvesting and electroluminescent properties.[27] In the course of this study, we found that a third-generation Cz dendrimer with a triazine core self-assembles into polycrystalline solids.[25] To our surprise, these crystals maintained their structural integrity even after the removal of the included solvent molecules, affording a non-solvated microporous framework. Nonetheless, their morphology was unsatisfactory for laser optics applications.

Herein, we present a family of dendrimers that form single-crystalline laser resonators. We newly design aromatic dendrimers G*n*COPV2 ($n = 1$–3) by introducing branched Cz dendrons to a highly fluorescent laser dye, carbon-bridged oligo(phenylenevinylene) (COPV2). Contrary to the conventional dendrimers, slow precipitation of G*n*COPV2 from their solutions affords crystalline solids. The crystallinity is high enough to be applied to single-crystal X-ray structure analysis. The Cz dendrons work as light-harvesting antennas that absorb non-polarized light and transfer it into the fluorescent COPV2 core, generating a polarized emission along the longer axis of the core. Upon strong optical pumping, these microcrystals display amplified spontaneous emission (ASE) and lasing without noticeable mechanical and optical degradation. The lasing properties were closely related to the morphology of the crystals and the orientation of the COPV2 moiety.

G1COPV2 bears two N-substituted Cz units on both termini of a COPV2 moiety with four phenyl and four *n*-octylphenyl substituents for sterically protecting and solubilizing groups (Figure 1 a). G2COPV2 and G3COPV2 comprise a COPV2 core carrying two multi-branched Cz dendrons with *t*-butyl groups at the outermost Cz units (Figure 1 a). The Cz dendrons and COPV2 core were synthesized according to previous studies[27–30] and were connected together via Pd-catalyzed amination reaction. Molecular structures of G*n*COPV2 were characterized by ^{1}H NMR spectroscopy (Supporting Information, Figures S1–S6) and mass spectrometry (Supporting Information, Figures S7–S9).

Figure 1 b shows electronic absorption and photoluminescence (PL) spectra of $CHCl_3$ solutions of G*n*COPV2. The absorption spectra display two series of absorption bands at 310–360 and 380–460 nm, which correspond to the S_0-S_1 transitions of the Cz dendron[31] and COPV2 units,[32,33] respectively. In contrast, upon excitation at 290 nm, PL spectra display PL bands only from the COPV2 unit at 430–550 nm, involving 0–0, 0–1, and 0–2 vibronic structures of COPV2.[34] The absence of PL from the Cz units indicates intramolecular energy transfer from the Cz dendrons to the COPV2 core (for PL properties with direct excitation of the COPV2 core; Supporting Information, Figure S10 and Table S1). The efficient energy transfer was anticipated because the fluorescence band of Cz and the absorption band of COPV2 overlap substantially.[26,29]

G*n*COPV2 readily precipitated into powdery solids through a slow diffusion of a nonsolvent vapor into the solution. As shown in the Supporting Information, Figure S11, G1COPV2 precipitated under all solvent/nonsolvent conditions examined, yielding well-defined polygonal microrods. Powder X-ray diffraction (PXRD) patterns display distinct peak sets, characteristic of polycrystals (Supporting Information, Figure S12). Analogously, G2COPV2 formed crystalline solids except for the case with a $CHCl_3$/MeOH combination in which amorphous spherical aggregates formed (Supporting Information, Figures S13 and S14). Interestingly, even the third-generation dendrimer G3COPV2 with a molecular weight as large as 4599 g mol^{-1} formed crystalline solid in 4 out of 8 solvent/nonsolvent conditions (Supporting Information, Figure S15). The resultant transparent polygonal grains display weak but distinguishable peaks in the PXRD profiles, indicating that these micrograins are substantially in a crystalline state (Supporting Information, Figure S16).

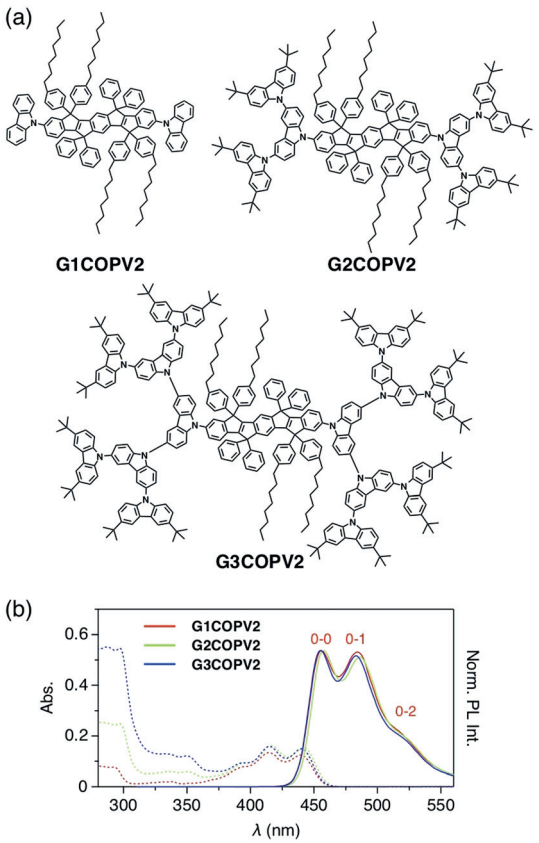

Figure 1. a) Molecular structures of G*n*COPV2 ($n = 1$–3). b) Electronic absorption (2.0 μM, in $CHCl_3$, dashed curves) and normalized PL ($\lambda_{ex} = 290$ nm, 2.0 μM, in $CHCl_3$, solid curves) spectra of G*n*COPV2 ($n = 1$–3). The vibrational levels of each PL band are denoted in red numbers.

In optimum precipitation conditions, flawless crystals of G*n*COPV2 were obtained, which were suitable for single-crystal X-ray structure analysis (for details, see the Supporting Information). Rod-shaped crystals of G1COPV2 adopt a space group of $P2_1/c$ and contain $CHCl_3$ and MeCN molecules as solvents of crystallization (Figure 2 a; Supporting Information, Figure S17, Table S2). The dihedral angle between COPV2 and adjacent Cz is 59.84°. G1COPV2

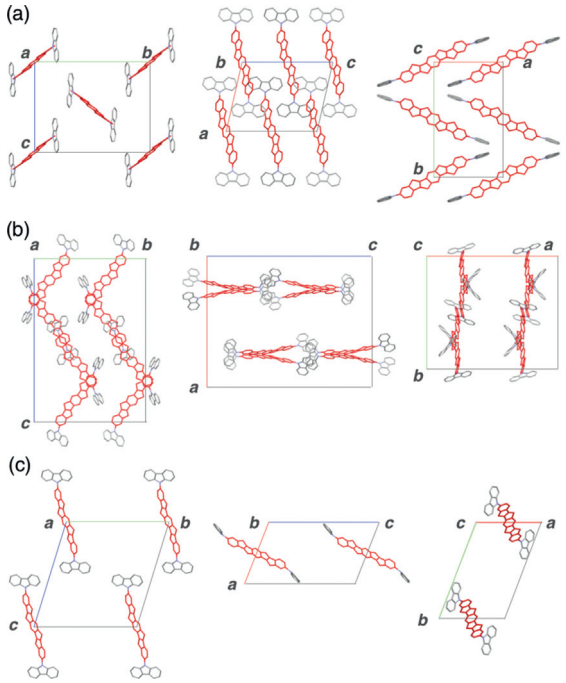

Figure 2. Crystal structures of a) G1COPV2, b) G2COPV2, and c) G3COPV2, viewed along the crystallographic *a*, *b*, and *c* axes. The peripheral moieties other than the COPV2 core and adjacent Cz units are omitted for clarity. The COPV2 core is colored in red.[37]

molecules contact with each other dominantly via multiple intermolecular C–H···π interactions (Supporting Information, Figure S17c). G2COPV2 forms a platelet crystallite with a space group of *Pbca* (Figure 2b; Supporting Information, Figure S18, Table S3). The crystal of G3COPV2 adopts a space group $P\bar{1}$ (Figure 2c; Supporting Information, Figure S19, Table S4). Remarkably, to the best of our knowledge, G3COPV2 is the largest purely organic dendrimer ever analyzed by single-crystal X-ray crystallography in terms of the molecular weight, while several metal–organic dendrimers with molecular weights heavier than G3COPV2 have been reported together with their single-crystal structures.[35,36]

The excellent crystallinity of G*n*COPV2 is attributed to two distinct structural features of the Cz dendrons. First, N-substituted Cz is a highly planar and rigid molecular unit, which is favorable for decreasing the entropic loss upon crystallization. Second, the branches were introduced at the 3- and 6-positions of Cz so that Cz can maintain its C_{2v} symmetry. Such relatively high structural symmetry is favorable for assembling into crystalline solids because it suppresses the entropic loss upon crystallization.

To investigate fluorescence and lasing properties, the size and shape of the microcrystals were further optimized (for details, see the Supporting Information). The morphologies of the resultant microcrystals were visualized by scanning electron microscopy (SEM, Figure 3d, f, and h) and fluorescence microscopy (FM, Figure 3j–l). The crystalline monodomain nature was confirmed by polarized optical microscopy (POM), where the brightness and contrast of the microcrystals under cross-polarized condition are highly dependent on the in-plane rotation of the sample (Supporting Information, Figures S20–S22).

The molecular alignment in these crystals was assigned based on the single-crystal X-ray analysis (Supporting Information, Figures S17–S19). In the rod-shaped microcrystal of G1COPV2, the crystallographic *a* axis (or [100] direction) orients parallel to the longer axis of the microrod (Figure 3e). Therein, COPV2 cores align almost parallel to the crystallographic [100] direction in a zigzag manner (Figure 3a). In contrast, the π-planes of G2COPV2 and G3COPV2 are nearly orthogonal to the longer axes of the microcrystals (Figure 3b and c), which, respectively coincide with their crystallographic *a* axis ([100] direction, Figure 3g) and *b* axis ([010] direction, Figure 3i).

Since the COPV2 cores are uni/bidirectionally aligned in the microcrystals of G*n*COPV2, the polarization profiles of their emission upon excitation of the COPV2 core with non-polarized light (λ_{ex} = 460–495 nm) exhibited polarization anisotropy along the alignment of the COPV2 cores (Figure 3m–o, blue). Here, 0° of the analyzer and polarizer was set to coincide with the [100] (for G1COPV2 and G2COPV2) or [010] (for G3COPV2) directions of the microcrystals. Virtually identical profiles are obtained for all the G*n*COPV2 microcrystals when the Cz units were excited with non-polarized light (λ_{ex} = 350–390 nm) because of the energy transfer from Cz to COPV2 (Figure 3m–o, green). Then, we utilize polarized excitation light and detect the emission intensities while rotating the polarizer. Emission profiles upon excitation of COPV2 cores (λ_{ex} = 460–495 nm) exhibit anisotropy along the COPV2 cores (Figure 3m–o, orange). On the other hand, the emission profiles upon excitation of Cz units (λ_{ex} = 350–390 nm) exhibit much less anisotropy for G2COPV2 and G3COPV2 (Figure 3m–o, red). These results indicate that the omnidirectionally oriented Cz units of G2COPV2 and G3COPV2 absorb incident light with little preference of the polarization angle. Meanwhile, the Cz units of G1COPV2 align unidirectionally in the crystal and only light with a suitable polarization direction is absorbed, leading to the emission anisotropy.

These microcrystals were subjected to photoexcitation with a femtosecond (fs) pulse laser (λ_{ex} = 397 nm, pulse width: 300 fs, repetition rate: 1 kHz, in detail, see the Supporting Information, Figure S23). Upon strong pumping, the facets or edges of the crystals emit green luminescence (Figure 4a–c insets). Upon pumping a microcrystal of G1COPV2 with a pumping intensity (P) of 369 μJ cm^{-2}, a set of prominent PL peaks emerges at around 488 nm with the broad PL band, which originates from the 0–1 vibrational band of G1COPV2 (Figure 4a). The observed sharp and broad PL lines are attributed to stimulated emission and ASE, respectively. A plot of the PL intensity at 488 nm versus P displays a nonlinear profile with a lasing threshold (P_{th}) at 318 μJ cm^{-2} (Figure 4d). As the size of the microcrystal increases, the free spectral range decreases with a linear correlation with the inverse of the crystal length (Supporting Information, Figure S24).

Analogous lasing behavior was observed for crystals of G2COPV2 and G3COPV2 with P_{th} of 66 and 293 μJ cm^{-2}, respectively (Figures 4b, c, e, f; Supporting Information, Figures S24, S25). The marked difference of the P_{th} values for G*n*COPV2 is attributed to two factors: 1) a difference of the COPV2 orientation in the crystallites, and 2) optical leakage

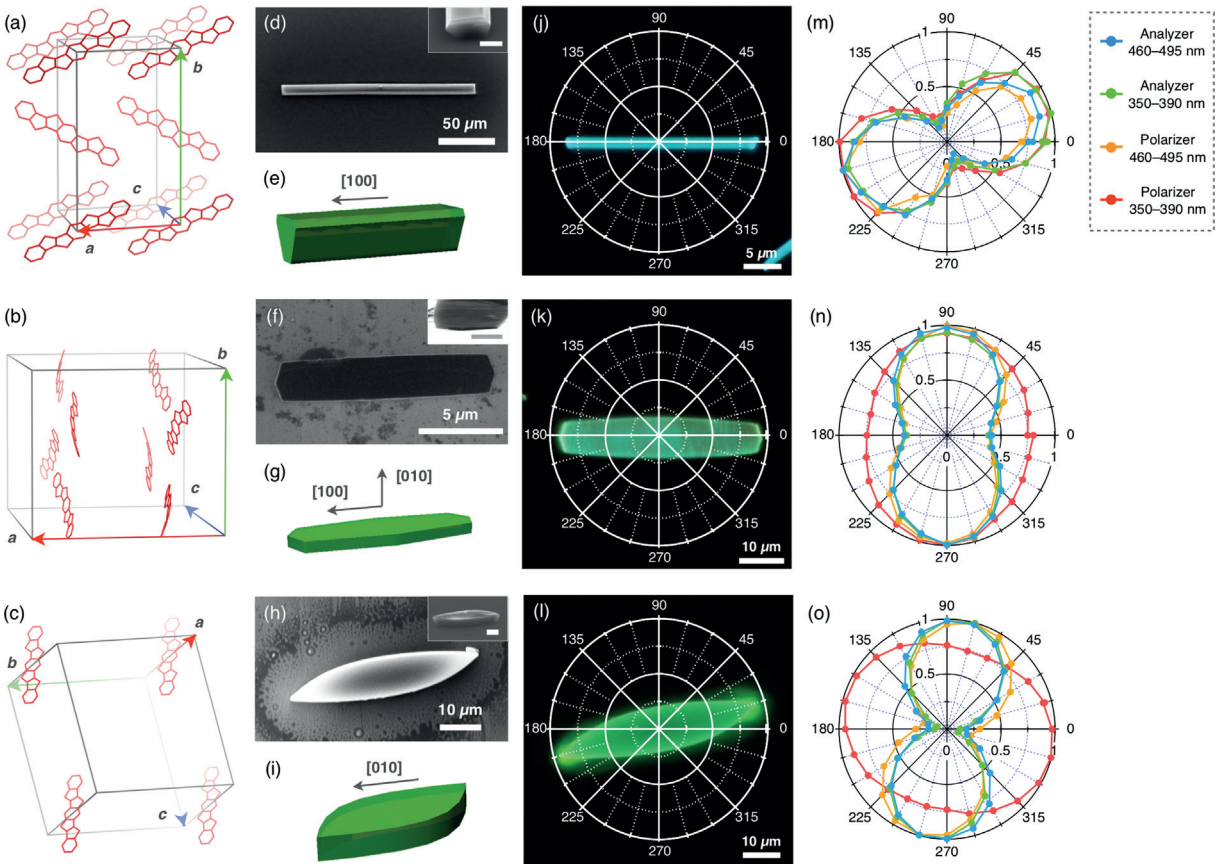

Figure 3. a)–c) Molecular orientation of the COPV2 cores in the microcrystals of G1COPV2 (a), G2COPV2 (b), and G3COPV2 (c). d)–i) SEM images and schematic representations of the microcrystals of G1COPV2 (d, e), G2COPV2 (f, g), and G3COPV2 (h, i) with arrows indicating crystallographic directions. Scale bars in insets: 10 μm. j)–l) FM images of the microcrystals of G1COPV2 (j), G2COPV2 (k), and G3COPV2 (l). m)–o) Plots of polarization-dependent normalized gray values of the luminescence intensity for microcrystals of G1–G3COPV2 in (j–l), respectively. The analyzer angle-dependent emission intensities were plotted upon excitation with non-polarized light at 460–495 nm (blue) and 350–390 nm (green), while the polarizer angle-dependent emission intensities were plotted upon excitation with polarized light at 460–495 nm (orange) and 350–390 nm (red).

at the crystal edges. For efficient light confinement in a rod-like crystal with counter end facets, an orthogonal orientation of the π-plane of COPV2 with the longer axis of the crystallites is preferable. As revealed by X-ray structure analysis, the π-plane of the COPV2 cores orient parallel to the longer axis direction in the G1COPV2 crystal (Figure 3a) while it is orthogonal in the G2COPV2 (Figure 3b) and G3COPV2 crystals (Figure 3c). Therefore, the comparatively high P_{th} for G1COPV2 is attributed to its unfavorable molecular orientation.

We investigated the optical pathways and the degree of light leakage by the two-dimensional finite-difference time-domain (2D-FDTD) simulations (Supporting Information, Figures S26 and S27). The simulated electric field distribution in the microrod crystal of G1COPV2 suggests a Fabry–Pérot (F-P) mode resonance (Figure 5a). Therein, a certain degree of confined light leaks at both end facets. On the other hand, the electric field distribution in the platelet crystal of G2COPV2 displays a bow-tie mode, where light inside the crystal is diagonally reflected at the crystal facets (Figure 5b). Such diagonal reflection drastically suppresses the light leakage and thereby contributes to the facile lasing with low P_{th}. The microcrystal of G3COPV2 displays whispering gallery mode (WGM) characteristics along the one side of the crystal curvature and exhibit orthogonal reflection at the crystal edges when a light source is located at the upper periphery (Figure 5c, in details, see the Supporting Information, Figure S26). The light confinement efficiency of G3COPV2 is even worse when the light source is located at the center of the crystal (Figure 5d; Supporting Information, Figure S26).

The light leakage from the microcrystals was further supported qualitatively by microscopic observations upon local excitation with a focused laser ($\lambda_{ex} = 450$ nm, Figure 5e,f). When the center of the microcrystal of G3COPV2 was excited, the luminescent light leaks substantially at the crystalline edges (Figure 5f). In contrast, when the center of the microcrystal of G2COPV2 was excited, the two end facets glowed moderately (Figure 5e), indicating that light is confined much more efficiently in the microcrystal of G2COPV2 than in that of G3COPV2. The high confinement efficiency, together with the preferable molecular orientation, contributes to the lowest P_{th} of the microcrystal of G2COPV2 among G*n*COPV2 (Supporting Information, Figure S25).

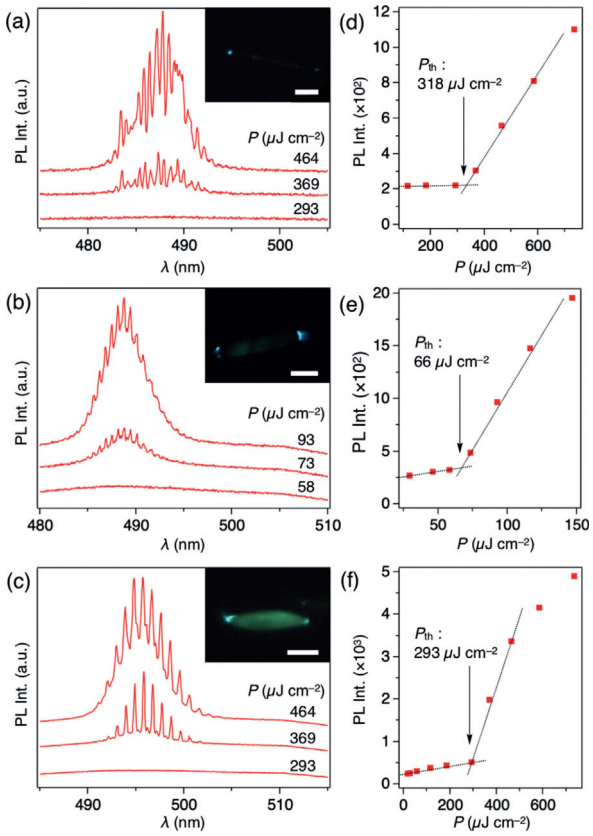

Figure 4. a)–c) PL spectra of G1COPV2 (a), G2COPV2 (b), and G3COPV2 (c) upon fs pumping with different pumping intensities (*P*). Insets show FM images upon fs pumping at 397 nm. Scale bars in insets: 20 μm. d)–f) Plots of PL intensities of G1COPV2 at 488 nm (d), G2COPV2 at 488 nm (e), and G3COPV2 at 496 nm (f) versus *P*.

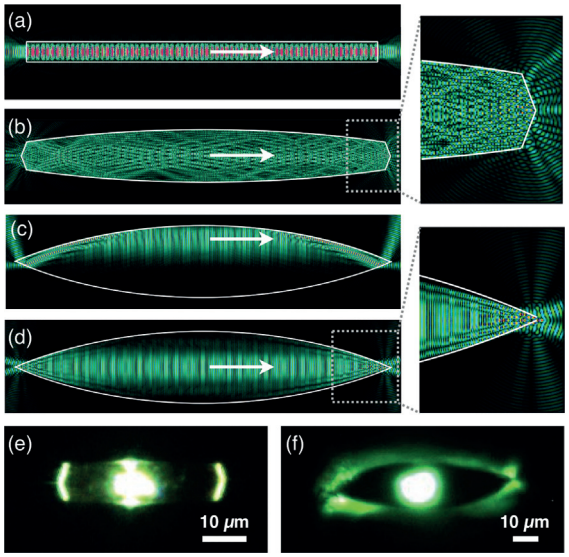

Figure 5. a)–d) Simulated electric field distributions in microcrystals of G1COPV2 (a), G2COPV2 (b), and G3COPV2 (c and d). The white arrows indicate the light source vectors. e),f) FM images of microcrystals of G2COPV2 (e) and G3COPV2 (f) upon excitation at the center of the crystal with a focused cw laser (λ_{ex} = 450 nm).

In conclusion, we synthesized a dendrimer family featuring high crystallinity, applicable to single-crystal X-ray structure analysis. It is noteworthy that the third-generation dendrimer with a molecular weight as high as 4600 g mol^{-1} is the largest organic dendrimer ever analyzed by single-crystal X-ray analysis. The excellent crystallinity of G*n*COPV2 is attributed to the Cz units that have high rigidity and planar morphology with C_{2v} symmetry. The obtained microcrystals were robust enough against optical pumping. The emission polarization, lasing properties, and light confinement modes tightly couple with the alignment of the constituent dendrimers and the morphology of the crystals. The present research opens up new applications of dendrimers in a field of laser optics.

Acknowledgements

The authors acknowledge Prof. Tatsuya Nabeshima and Prof. Takashi Nakamura in University of Tsukuba for PL quantum yield experiments and Eri Hisamura in Kyushu University for MALDI-TOF MS experiments. This work was supported by a Grant-in-Aid for Scientific Research on Innovative Areas "π-System Figuration" (JP17H05142, JP17H05163, JP17H05146), "Aquatic Functional Materials" (JP19H05716), Scientific Research (A) (JP16H02081), Scientific Research (B) (JP16H04106, JP20H02801), Scientific Research (S) (JP15H05757), and Young Scientist (JP19K15334) from Japan Society for the Promotion of Science (JSPS), ERATO Yamamoto Atom-Hybrid Project (JPMJER1503) from Japan Science and Technology Agency (JST), Cooperative Research Program of "Network Joint Research Center for Materials and Devices", The Ogasawara Foundation for the Promotion of Science & Technology, The Kao Foundation for Arts and Sciences, University of Tsukuba Pre-strategic initiative "Ensemble of light with matters and life", and TIA Kakehashi.

Conflict of interest

The authors declare no conflict of interest.

Keywords: dendrimers · laser chemistry · light harvesting · microcavities · photochemistry

[1] I. D. W. Samuel, G. A. Turnbull, *Chem. Rev.* **2007**, *107*, 1272–1295.
[2] G.-Q. Wei, X.-D. Wang, L.-S. Liao, *Adv. Funct. Mater.* **2019**, *29*, 1902981.
[3] A. J. C. Kuehne, M. C. Gather, *Chem. Rev.* **2016**, *116*, 12823–12864.
[4] Y. Cui, J. Zhang, H. He, G. Qian, *Chem. Soc. Rev.* **2018**, *47*, 5740–5785.
[5] W. Zhang, J. Yao, Y. S. Zhao, *Acc. Chem. Res.* **2016**, *49*, 1691–1700.
[6] R. Medishetty, J. K. Zareba, D. Mayer, M. Samoć, R. A. Fischer, *Chem. Soc. Rev.* **2017**, *46*, 4976–5004.

[7] M. Ichikawa, R. Hibino, M. Inoue, T. Haritani, S. Hotta, K. Araki, T. Koyama, Y. Taniguchi, *Adv. Mater.* **2005**, *17*, 2073 – 2077.
[8] H. Mizuno, U. Haku, Y. Marutani, A. Ishizumi, H. Yanagi, F. Sasaki, S. Hotta, *Adv. Mater.* **2012**, *24*, 5744 – 5749.
[9] H.-H. Fang, J. Yang, J. Feng, T. Yamao, S. Hotta, H.-B. Sun, *Laser Photonics Rev.* **2014**, *8*, 687 – 715.
[10] P. Guo, M. K. Hossain, X. Shen, H. Sun, W. Yang, C. Liu, C.-Y. Ho, C.-K. Kwok, S. Tsang, Y. Luo, J.-C. Ho, K.-M. Yu, *Adv. Opt. Mater.* **2017**, *6*, 993 – 996.
[11] W. Zhang, Y. Yan, J. Gu, J. Yao, Y. S. Zhao, *Angew. Chem. Int. Ed.* **2015**, *54*, 7125 – 7129; *Angew. Chem.* **2015**, *127*, 7231 – 7235.
[12] C. Zhang, C. L. Zou, H. Dong, Y. Yan, J. Yao, Y. S. Zhao, *Sci. Adv.* **2017**, *3*, e1700225.
[13] J. Zhao, Y. Yan, C. Wei, W. Zhang, Z. Gao, Y. S. Zhao, *Nano Lett.* **2018**, *18*, 1241 – 1245.
[14] K. Wang, W. Zhang, Z. Gao, Y. Yan, X. Lin, H. Dong, C. Zhang, W. Zhang, J. Yao, Y. S. Zhao, *J. Am. Chem. Soc.* **2018**, *140*, 13147 – 13150.
[15] G. Wang, W. Qin, L. Wang, G. Wei, P. Zhu, R. Kim, *Opt. Express* **2008**, *16*, 11907 – 11914.
[16] D. Astruc, E. Boisselier, C. Ornelas, *Chem. Rev.* **2010**, *110*, 1857 – 1959.
[17] K. Matsuoka, K. Albrecht, A. Nakayama, K. Yamamoto, K. Fujita, *ACS Appl. Mater. Interfaces* **2018**, *10*, 33343 – 33352.
[18] A. Adronov, J. M. J. Fréchet, *Chem. Commun.* **2000**, 1701 – 1710.
[19] C.-F. Li, F. Jin, X.-Z. Dong, W.-Q. Chen, X.-M. Duan, *J. Lumin.* **2007**, *127*, 321 – 326.
[20] F. Jin, C. F. Li, X. Z. Dong, W. Q. Chen, X. M. Duan, *Appl. Phys. Lett.* **2006**, *89*, 241101.
[21] J. R. Lawrence, E. B. Namdas, G. J. Richards, P. L. Burn, I. D. W. Samuel, *Adv. Mater.* **2007**, *19*, 3000 – 3003.
[22] C.-F. Li, X.-Z. Dong, F. Jin, W. Jin, W.-Q. Chen, Z.-S. Zhao, X. M. Duan, *Appl. Phys. A* **2007**, *89*, 145 – 148.
[23] R. E. Bauer, V. Enkelmann, U. M. Wiesler, A. J. Berresheim, K. Müllen, *Chem. Eur. J.* **2002**, *8*, 3858 – 3864.
[24] O. Lukin, D. Schubert, C. M. Müller, W. B. Schweizer, V. Gramlich, J. Schneider, G. Dolgonos, A. Shivanyuk, *Proc. Natl. Acad. Sci. USA* **2009**, *106*, 10922 – 10927.
[25] S. Nakajima, K. Albrecht, S. Kushida, E. Nishibori, T. Kitao, T. Uemura, K. Yamamoto, U. H. F. Bunz, Y. Yamamoto, *Chem. Commun.* **2018**, *54*, 2534 – 2537.
[26] K. Albrecht, K. Yamamoto, *J. Am. Chem. Soc.* **2009**, *131*, 2244 – 2251.
[27] K. Albrecht, K. Matsuoka, K. Fujita, K. Yamamoto, *Angew. Chem. Int. Ed.* **2015**, *54*, 5677 – 5682; *Angew. Chem.* **2015**, *127*, 5769 – 5774.
[28] K. Albrecht, K. Matsuoka, D. Yokoyama, Y. Sakai, A. Nakayama, K. Fujita, K. Yamamoto, *Chem. Commun.* **2017**, *53*, 2439 – 2442.
[29] X. Zhu, H. Tsuji, J. T. López Navarrete, J. Casado, E. Nakamura, *J. Am. Chem. Soc.* **2012**, *134*, 19254 – 19259.
[30] H. Tsuji, E. Nakamura, *Acc. Chem. Res.* **2019**, *52*, 2939 – 2949.
[31] Z. Wei, J. Xu, G. Nie, Y. Du, S. Pu, *J. Electroanal. Chem.* **2006**, *589*, 112 – 119.
[32] M. Morales-Vidal, P. G. Boj, J. M. Villalvilla, J. A. Quintana, Q. Yan, N. T. Lin, X. Zhu, N. Ruangsupapichat, J. Casado, H. Tsuji, E. Nakamura, M. A. Díaz-García, *Nat. Commun.* **2015**, *6*, 8458.
[33] M. Morales-Vidal, J. A. Quintana, J. M. Villalvilla, P. G. Boj, H. Nishioka, H. Tsuji, E. Nakamura, G. L. Whitworth, G. A. Turnbull, I. D. W. Samuel, M. A. Díaz-García, *Adv. Opt. Mater.* **2018**, *6*, 1800069.
[34] D. Okada, S. Azzini, H. Nishioka, A. Ichimura, H. Tsuji, E. Nakamura, F. Sasaki, C. Genet, T. W. Ebbesen, Y. Yamamoto, *Nano Lett.* **2018**, *18*, 4396 – 4402.
[35] K. Omoto, N. Hosono, M. Gochomori, K. Albrecht, K. Yamamoto, S. Kitagawa, *Chem. Commun.* **2018**, *54*, 5209 – 5212.
[36] J. W. Kriesel, S. König, M. A. Freitas, A. G. Marshall, J. A. Leary, T. D. Tilley, *J. Am. Chem. Soc.* **1998**, *120*, 12207 – 12215.
[37] CCDC 2004039, 2004041, and 2004040 (G1COPV2, G2COPV2, and G3COPV2) contain the supplementary crystallographic data for this paper. These data are provided free of charge by The Cambridge Crystallographic Data Centre.

Manuscript received: January 15, 2020
Revised manuscript received: April 9, 2020
Accepted manuscript online: April 27, 2020
Version of record online: May 20, 2020

